SCIENCE CHINA
Chemistry

• ARTICLES •
• SPECIAL ISSUE • Organic photovoltaics

February 2015 Vol.58 No.2: 323–330
doi: 10.1007/s11426-014-5218-4

Alcohol/water-soluble porphyrins as cathode interlayers in high-performance polymer solar cells

Tao Jia, Weilong Zhou, Fenghong Li, Yajun Gao, Lu Wang, Jianxiong Han, Jingying Zhang* & Yue Wang

State Key Laboratory of Supramolecular Structure and Materials, Jilin University, Changchun 130012, China

Received June 28, 2014; accepted July 21, 2014; published online December 31, 2014

Three alcohol/water-soluble porphyrins, Zn-TPyPMeI: zinc(II) *meso*-tetra(*N*-methyl-4-pyridyl) porphyrin tetra-iodide, Zn-TPyPAdBr: zinc(II) *meso*-tetra[1-(1-adamantylmethyl ketone)-4-pyridyl] porphyrin tetra-bromide and MnCl-TPyPAdBr: manganese(III) *meso*-tetra[1-(1-adamantylmethyl ketone)-4-pyridyl] porphyrin tetra-bromide were employed as cathode interlayers to fabricate polymer solar cells (PSCs). The $PC_{71}BM$ ([6,6]-phenyl C_{71} butyric acid methyl ester) and PCDTBT (poly[*N*-9″-hepta-decanyl-2,7-carbazole-*alt*-5,5-(4′,7′-di-2-thienyl-2′,1′,3′-benzothiadiazole)])-blend films were used as active layers in polymer solar cells (PSCs). The PSCs with alcohol/water-soluble porphyrins interlayer showed obviously higher power conversion efficiency (PCE) than those without interlayers. The highest PCE, 6.86%, was achieved for the device with MnCl-TPyPAdBr as an interlayer. Ultraviolet photoemission spectroscopic (UPS), carrier mobility, atomic force microscopy (AFM) and contact angle (θ) characterizations demonstrated that the porphyrin molecules can result in the formation of interfacial dipole layer between active layer and cathode. The interfacial dipole layer can obviously improve the open-circuit voltage (V_{oc}) and charge extraction, and sequentially lead to the increase of PCE.

polymer solar cells, cathode interlayer, alcohol/water-soluble porphyrins

1 Introduction

Bulk heterojunction (BHJ) solar cells based on active layers comprised of conjugated polymers and fullerenes have attracted great attention and are considered as promising devices for an alternative energy source because of their light weight, low cost, and flexibility [1,2]. The power-conversion efficiency (PCE) of polymer solar cells (PSCs) larger than 9% has been achieved [3,4].

To improve the PCE of PSCs, great deal of effort has been invested in the synthesis of new materials [5–9], device structure optimization [10,11], and morphology modification of active layers [12]. Moreover, studies on the interface between electrodes and active layers have been devoted to improving device efficiency by decreasing charge collection/extraction barriers and forming ohmic contact between electrode and active layer. Significant improvements of PCE by placing a cathode interlayer between the active layer and the metal electrode have been realized. It is worth noting that certain alcohol/water-soluble organic or polymeric electrolytes used as cathode interlayers can strongly enhance the PCE of PSCs. Compared to other cathode-interfacial-layer materials, the advantages of alcohol/water-soluble organic or polymeric materials for PSCs are remarkable due to their simple, vacuum-free, and environmental friendly film formation during device fabrication [3,4,13–17]. So far, most of the cathode interlayers with high efficiency have been composed of polymers; small organic molecule-based cathode interlayers that can efficiently improve the performance of PSCs have been rare [18–20]. Compared to polymers, the advantages of small

*Corresponding author (email: zhangjingy@jlu.edu.cn)

molecules lie in their well-defined structures, consistent high purity, and capacity for modification [21].

As a family of functional molecules, porphyrins have important roles in both natural and synthesized systems due to their excellent photophysical, semiconducting, electrochemical, and catalytic properties, as well as their stability [22–27]. Recent investigations have focused on the applications of porphyrin-based materials in organic electronic devices such as organic light-emitting devices (OLEDs) [28,29], organic photovoltaic devices (OPV) [30–37], organic field-effect transistors (OFETs) [38]. So far, in most of these studies, the porphyrin compounds were applied to active layers in organic electronic devices; their application beyond active materials has been very limited [20]. Therefore, exploration of the new applications and functions of porphyrins in organic electronic devices shows great potential. In this contribution, several alcohol/water-soluble porphyrin molecules (Scheme 1) were employed as cathode interlayers, which led to significant improvement of the performance of polymer solar cells (PSCs).

2 Experimental

2.1 Synthesis and characterization

^{1}H NMR spectra were measured on a Varian Mercury 300 MHz spectrometer (USA) with tetramethylsilane as the internal standard. Elemental analyses were performed on a flash EA 1112 spectrometer (Elementar, Germany). All reagents and solvents, unless otherwise specified, were obtained from Aldrich (USA) and Acros (Belgium) and used as received. PCDTBT (Lot #YY6092C) was purchased from 1-material Chemscitech Inc. (Canada). $PC_{71}BM$ (Lot #14A0021E1) was purchased from American Dye Source (USA). All reactions were carried out using Schlenk techniques under a nitrogen atmosphere.

2.1.1 Synthesis of zinc(II) *meso*-tetra(4-pyridyl) porphine (Zn-TPyP)

H2-TPyP (200 mg, 0.32 mmol), zinc acetate (550 mg, 3 mmol) were dissolved in 500 mL dry DMF. Under nitrogen atmosphere, the solution was stirred and heated to reflux for 5 h. After being cooled to room temperature, the solvent was removed by vacuum evaporation; the crude product was purified by alumina oxide chromatography with an eluent chloroform; and a purple powder was obtained. Yield: 131 mg (60%). ^{1}H NMR (300 MHz, DMSO-d_6): δ 9.02 (d, J=6.0 Hz, 8 H), 8.85 (s, 8 H), 8.21 (d, J=6.0 Hz, 8 H). Anal. calcd: C 70.44%, H 3.55%, N 16.43%; found: C 70.87%, H 3.36%, N 16.49%.

2.1.2 Synthesis of zinc(II) *meso*-tetra(*N*-methy-4-pyridyl) porphine tetra-iodide (Zn-TPyPMeI)

A solution of Zn-TPyP (200 mg, 0.29 mmol) and methyl

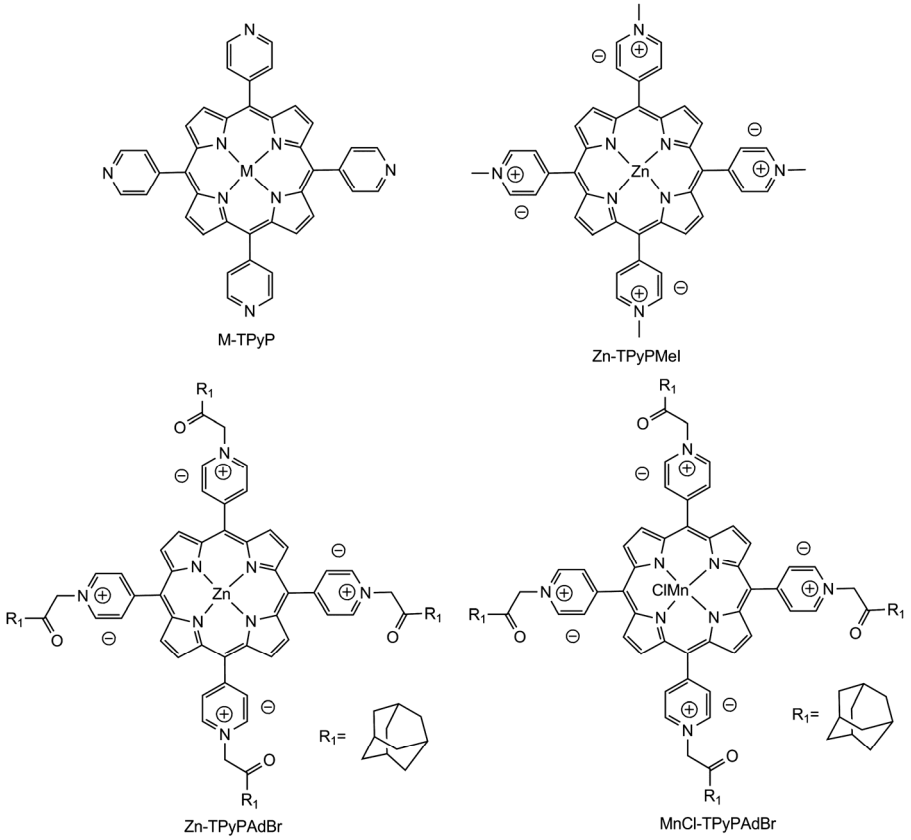

Scheme 1 The structures of alcohol/water soluble porphyrins.

iodide (850 mg, 6 mmol) in 30 mL dry DMF was heated at 100 °C for 10 h. After being cooled to room temperature, the solvent was removed by vacuum evaporation and the crude product was purified by recrystallization with methanol and chloroform to obtain a black-brown powder. Yield: 343 mg (95%). ^{1}H NMR (300 MHz, DMSO-d_6): δ 9.43 (d, J=6.6 Hz, 8 H), 9.10 (s, 8 H), 8.92 (d, J=6.6 Hz, 8 H), 4.73 (s, 12 H). Anal. calcd: C 42.28%, H 2.90%, N 8.97%; found: C 42.18%, H 2.88%, N 8.85%.

2.1.3 Synthesis of zinc(II) *meso*-tetra[1-(1-adamantylmethyl ketone)-4-pyridyl]porphyrin tetra-bromide (Zn-TPyPAdBr)

A solution of Zn-TPyP (200 mg, 0.29 mmol) and 1-adamantyl bromomethyl ketone (447 mg, 1.74 mmol) in 30 mL dry DMF was heated at 100 °C for 12 h. After being cooled to room temperature, the solvent was removed by vacuum evaporation and the crude product was purified by recrystallization with methanol and chloroform to obtain a black-brown powder. Yield: 445 mg (90%). ^{1}H NMR (300 MHz, DMSO-d_6):δ 9.35 (d, J=6.6 Hz, 8 H), 9.07 (m, 24 H), 6.40 (s, 8 H), 2.18 (s, 12 H), 2.13 (s, 24 H), 1.83 (s, 24 H). Anal. calcd: C 61.78%, H 5.42%, N 6.55%; found: C 61.87%, H 5.36%, N 6.49%.

2.1.4 Synthesis of manganses(III) *meso*-tetra(4-pyridyl) porphine (MnCl-TPyP)

H2-TPyP (200 mg, 0.32 mmol) and manganese (II) chloride (234 mg, 1.86 mmol) were dissolved in 500 mL dry DMF. Under nitrogen atmosphere, the solution was stirred and heated to reflux for 8 h. After being cooled to room temperature, the solvent was removed by vacuum evaporation and the crude product was purified by alumina oxide chromatography with an eluent chloroform to obtain a brown powder. Yield: 163 mg (72%). Anal. calcd: C 67.95%, H 3.42%, N 15.85%; found: C 67.98%, H 3.39%, N 15.84%.

2.1.5 Synthesis of manganese(III) *meso*-tetra[1-(1-adamantylmethyl ketone)-4-pyridyl] porphyrin tetra-bromide (MnCl-TPyPAdBr)

A solution of MnCl-TPyP (200 mg, 0.28 mmol) and 1-adamantyl bromomethyl ketone (437 mg, 1.7 mmol) in 30 mL dry DMF was heated at 100 °C for 12 h. After being cooled to room temperature, the solvent was removed by vacuum evaporation and the crude product was purified by recrystallization with methanol and chloroform to obtain a brown powder. Yield: 426 mg (88%). Anal. calcd: C 60.89%, H 5.34%, N 6.46%; found: C 60.87%, H 5.36%, N 6.49%.

2.2 Device fabrication

The ITO glass substrates were precleaned carefully and treated with plasma for 7 min. The blend ratio of PCDTBT:$PC_{71}BM$ is 1:4 by weight and the active layer (35 mg/mL) was spin-cast from a mixed solvent of chlorobenzene/o-dichlorobenzene (ratio=1:3). Porphyrins were dissolved in water. First, PEDOT:PSS (Baytron PVP Al 4083) was spin-coated onto a cleaned ITO and annealed in air at 120 °C for 10 min. Second, blend films of PCDTBT:$PC_{71}BM$ were spin-cast from a solution of PEDOT:PSS and then annealed in a glove box at 75 °C for 10 min. About 5 nm of cathode interlayer was deposited onto the active layer by spin-coating a porphyrin water solution (0.4 mg/mL); next 100 nm Al was evaporated as a cathode. For the electron-only devices, Al was vacuum-deposited onto cleaned ITO as an anode. Then the same procedures for the fabrication of polymer solar cells described above were followed to complete the counterparts. The active area of each device was 2.5×2.0 mm^2.

2.3 Device characterizations

The current-density voltage (J-V) characteristics of the devices were measured under N_2 atmosphere in the glove box by using a Keithley 2400 (USA) both under illumination and in the dark. The J-V and external quantum efficiency (EQE) characteristics of all the devices were measured on a Sciencetech (Canada) SSO-5K solar-spectrum-simulation and device-measurement system. The simulated solar light was calibrated to match 100 mW/cm^2 AM 1.5G level by a standard monocrystalline silicon solar cell. All devices were measured at ambient conditions. The J-V measurement software was programmed with National Instrument (NI) Labview 6.5 (USA) and the EQE was calculated directly by software received from Sciencetech (Canada). In addition, the static contact angles of the prepared surfaces were measured with a commercial contact-angle system (Data-Physics OCA 20, Germany) at ambient temperature using a 4 μL water droplet as the indicator. AFM images were measured with an S II Nanonaviprobe station 300 HV (Seiko, Japan) in contact mode.

3 Results and discussion

For comparison, two control devices were fabricated. One was based on the active layer without any treatment. The active layer of the other control device was treated with water, which is the solvent of porphyrins. The water treatment of the active layer was performed in a similar manner as was used for the fabrication of the devices with cathode interlayers. The contribution of the porphyrin rather than the solvent to the improvement of PSCs was thus revealed. PCDTBT:$PC_{71}BM$ blend films were employed as active layers to prepare a set of devices (Figure 1) with the following structures.

Device 1: [ITO/PEDOT:PSS/PCDTBT:$PC_{71}BM$/Al]

Device 2: [ITO/PEDOT:PSS/PCDTBT:$PC_{71}BM$/water/Al]

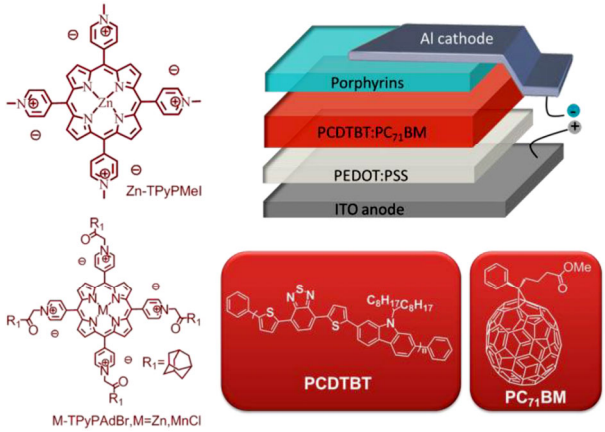

Figure 1 The structure of the PSC devices and the structures of materials used in these devices.

Device 3: [ITO/PEDOT:PSS/PCDTBT:PC_{71}BM/Zn-TPy-PMeI/Al]

Device 4: [ITO/PEDOT:PSS/PCDTBT:PC_{71}BM/Zn-TPy-PAdBr/Al]

Device 5: [ITO/PEDOT:PSS/PCDTBT:PC_{71}BM/MnCl-TPy-PAdBr/Al]

Figure 2 presents the current density versus voltage (*J*-*V*) characteristics of the devices under AM 1.5G illumination at 100 mW/cm^2 and in the dark. Figure 3 shows the external quantum efficiency (EQE). Table 1 summarizes the open circuit voltage (V_{oc}), short circuit (J_{sc}), fill factor (FF), power conversion efficiency (PCE), series resistance (R_s) and shunt resistance (R_{sh}) derived from the *J*-*V* characteristics under illumination.

The devices with different cathode interlayers show a V_{oc} of 0.896 V for Device 3, 0.916 V for Device 4, and 0.927 V for Device 5, which were higher than the control devices (V_{oc}=0.880 and 0.868 V for Device 1 and Device 2, respectively). The improvement of V_{oc} can be mainly attributed to the interlayer-induced decrease of work function (WF) of the Al cathode. Ultraviolet photoemission spectroscopic (UPS) measurements (Figure 4) demonstrated that the WF of Al decreased upon the introduction of the porphyrin layer onto the surface of the Al film. The WF values derived from the UPS of the Al surface treated by different cathode interlayers were 3.51 eV for Zn-TPyPMeI, 3.42 eV for Zn-TPyPAdBr, and 3.32 eV for MnCl-TPyPAdBr, whereas the *WF* of the bare Al was 4.2 eV. Therefore, it was concluded that porphyrin-based interlayers could lead to the WF decrease of the Al cathode. In addition, a MnCl-TPyPAdBr interlayer is more efficient for minimizing the WF of Al. Based on the electrochemical and absorption data the HOMO energy levels (−5.58 eV for Zn-TPyPMeI, −5.62 eV for Zn-TPyPAdBr and −5.70 eV for MnCl-TPyPAdBr) could be calculated.

The PCE for the devices with cathode interlayers were much higher than the control devices due to the simultaneous enhancement in V_{oc}, J_{sc}, and FF (Table 1). It is obvious

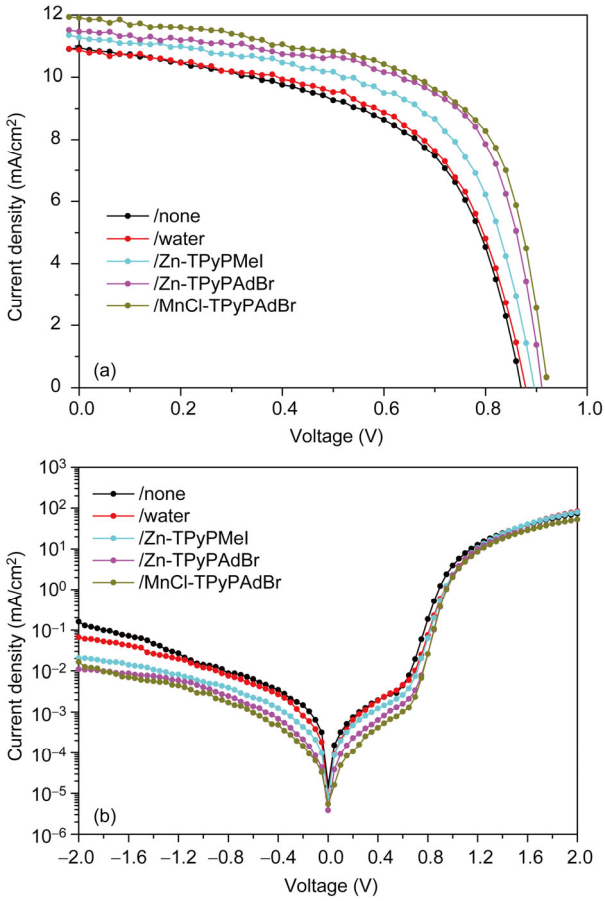

Figure 2 The effect of different cathodes on PSCs performance. (a) *J*-*V* characteristics of devices with the various cathodes at the surface of active layer under 100 W/m^2 AM 1.5G illumination; (b) *J*-*V* characteristics of the five devices in the dark.

Table 1 The performances of PCDTBT:PC_{71}BM PSCs with the various cathodes

Active layer treatment (Device-*n*)	V_{oc} (V)	J_{sc} (mA/cm^2)	FF (%)	PCE (%)	R_s (Ω cm^2)	R_{sh} (Ω cm^2)
None (Device-1)	0.868	10.95	56.2	5.34 (5.26)	15.7	505
Water (Device-2)	0.880	10.87	56.8	5.43 (5.40)	14.1	606
Zn-TPyPMeI (Device-3)	0.896	11.27	60.0	6.06 (6.04)	11.5	787
Zn-TPyPAdBr (Device-4)	0.916	11.47	63.6	6.68 (6.61)	7.1	968
MnCl-TPyPAdBr (Device-5)	0.927	11.91	62.1	6.86 (6.79)	5.4	980

that the introduction of porphyrins between the active layer and the Al cathode resulted in the improved PCE and the contribution from the solvent (water) to the PSCs was relatively smaller even though in Device 2, the solvent treatment slightly improved both the V_{oc} and FF. The resistances (R_s) and shunt resistances (R_{sh}) (Table 1) were derived from the *J*-*V* curves of the devices. Devices 3–5 with porphyrin interlayers had remarkably smaller R_s and larger R_{sh} compared with control Devices 1 and 2. Moreover, the mini-

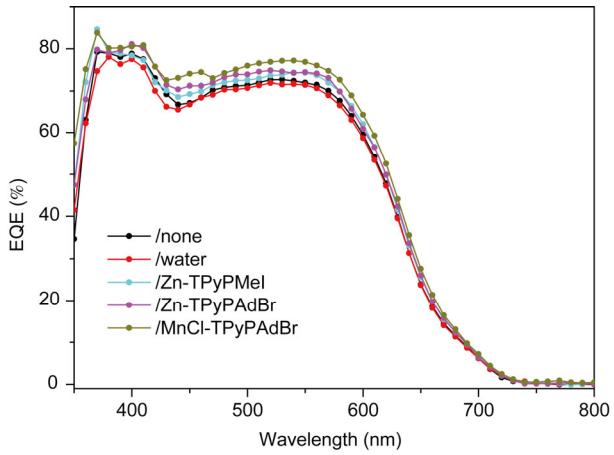

Figure 3 EQE spectra of Devices 1–5.

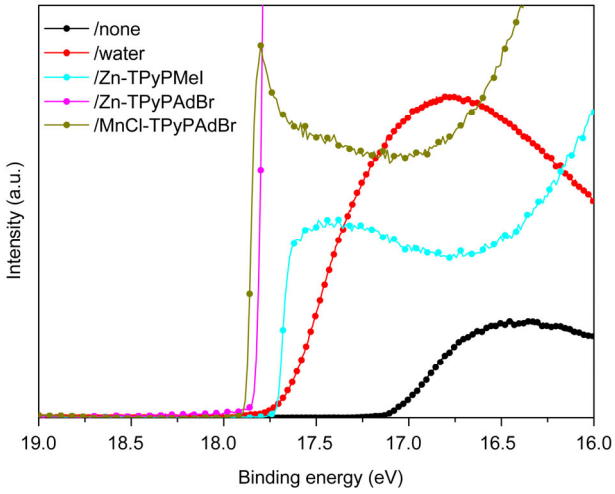

Figure 4 Ultraviolet photoelectron spectra of Al electrodes covered with series cathode interlayers within the range of 16–19 eV.

mal R_s (5.4 Ω cm^2) and maximal R_{sh} (980 Ω cm^2) were recorded for Device 5, which ensured that Device 5 had large J_{sc}. Device 5 with the MnCl-TPyPAdBr interlayer displayed the highest PCE value (6.86%).

The *J*-*V* characteristics of the devices obtained under dark conditions are presented in Figure 2(b). The dark current densities of Devices 3–5 with cathode interlayers were significantly suppressed, which implied that the built-in potential (V_{bi}) across the device, which is the upper limit of the attainable V_{oc} in PSCs, drastically increased upon the utilization of porphyrins cathode interlayers. Therefore, the increase of V_{bi} should be responsible for the increase in V_{oc} in the devices with porphyrins as cathode interlayers. Devices 3–5 displayed noticeably higher J_{sc} compared with control Devices 1 and 2. The improved PCE of the devices with the different cathode interlayers were consistent with the higher incident photon-to-current efficiency (IPCE) values, which can be higher than 80% (Figure 3). The J_{sc} values calculated from integration of the EQE spectra are 11.31 mA/cm^2 for Zn-TPyPMeI, 11.42 mA/cm^2 for Zn-TPyPAdBr and 11.82 mA/cm^2 for MnCl-TPyPAdBr, which are in agreement with the PCE obtained from *J*-*V* characteristics under illumination.

Simultaneous enhancement of V_{oc} and J_{sc} resulted in increase of FF for the optimized devices, which were 60.0% for Device 3, 63.6% for Device 4, and 62.1% for Device 5. The control Devices 1 and 2 showed much lower FF value (56.2% for Device 1 and 56.8% for Device 2). These results demonstrated that the introduction of a porphyrin interlayer improved the devices' charge transport and extraction abilities. To confirm this result, the *J*-*V* characteristics of single-charge carrier devices with the following structures were investigated:

Device 6: [ITO/Al/PCDTBT:$PC_{71}BM$/Al]

Device 7: [ITO/Al/PCDTBT:$PC_{71}BM$/water/Al]

Device 8: [ITO/Al/PCDTBT:$PC_{71}BM$/Zn-TPyPMeI/Al]

Device 9: [ITO/Al/PCDTBT:$PC_{71}BM$/Zn-TPyPAdBr/Al]

Device 10: [ITO/Al/PCDTBT: $PC_{71}BM$/MnCl-TPyPAdBr/Al]

As shown in Figure 5, Devices 8–10 with cathode interlayers displayed significantly higher current densities than Devices 6 and 7 without cathode interlayers. This result means that the devices with a cathode interlayer have better electron collection and transport properties. The electron mobility can be measured in the space charge limited current (SCLC) regime as described by Eq. (1):

$$J = 9\varepsilon_0\varepsilon_r\mu V^2 / 8L^3 \quad (1)$$

where ε_0 is the permittivity of free space; ε_r is the dielectric constant of the active layer; μ_0 is the zero-field mobility; V is the voltage drop across the device; and L is the active-layer thickness. The electron mobilities are 1.48×10^{-3} (Device 6), 1.65×10^{-3} (Device 7), 2.88×10^{-3} (Device 8), 7.64×10^{-3} (Device 9) and 6.80×10^{-3} cm^2/(V s) (Device 10). These results were in agreement with the increasing trend of FF in PSCs (Table 1).

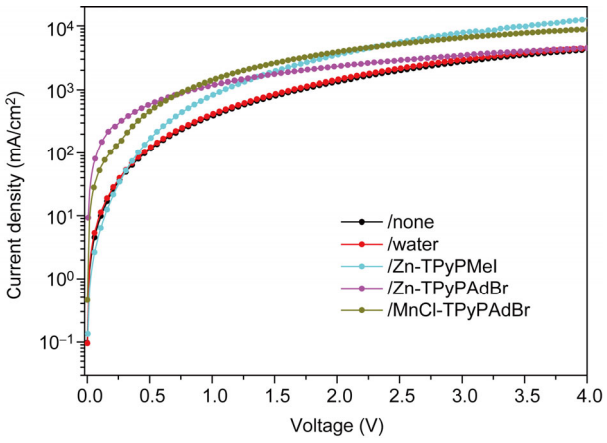

Figure 5 Experimental dark-current density-applied voltage (*J*-*V*) characteristics of electron-only devices for the various cathodes.

Figure 6(a1–e1) shows the surface-morphology images obtained with atomic-force microscopy (AFM) measurement at ambient conditions. The surface of the PCDTBT:$PC_{71}BM$ BHJ film is relatively smooth, with a root-mean-square (RMS) roughness of 0.89 nm (Figure 6(a1)). The water-treated surface was slightly smoother than the pristine film, with an RMS roughness of 0.78 nm, and remained homogeneous as shown in Figure 6(a2). Therefore, the improvement of V_{oc} and FF with water treatment is hardly related to the change of morphology. However, porphyrin-treated surfaces of PCDTBT:$PC_{71}BM$ blend films show a similar morphology. There are visible islands distributed over the surface due to the self-aggregation of porphyrin molecules and the RMS roughness are 1.36 nm for Zn-TPyPMeI, 1.20 nm for Zn-TPyPAdBr and 1.30 nm for MnCl-TPyPAdBr.

The surface polarity was studied by measuring the water-contact angle (θ) for the surfaces of PCDTBT:$PC_{71}BM$, PCDTBT:$PC_{71}BM$/water and PCDTBT:$PC_{71}BM$/porphyrins.

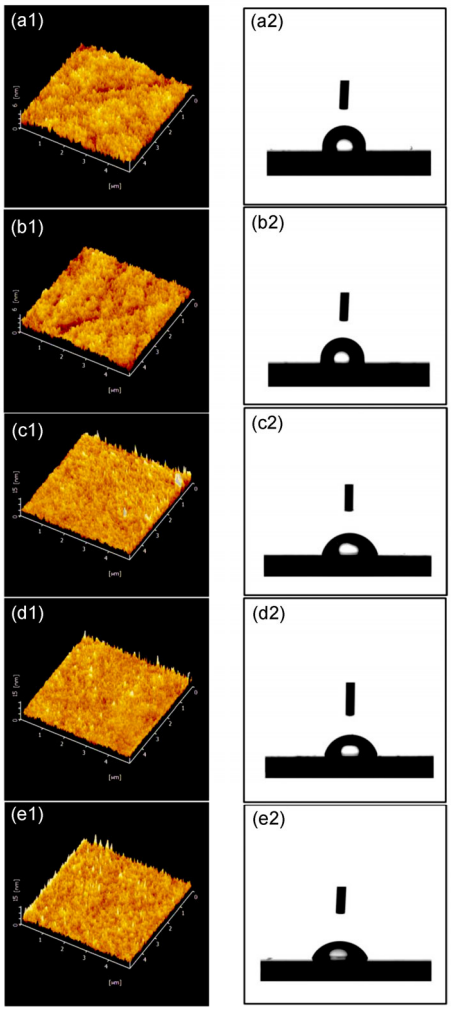

Figure 6 AFM images and photos of water droplets on the surfaces of (a) PCDTBT:$PC_{71}BM$ BHJ film, (b) PCDTBT:$PC_{71}BM$ BHJ film with water treatment, (c) Zn-TPyPMeI on PCDTBT:$PC_{71}BM$ BHJ film, (d) Zn-TPyPAdBr on PCDTBT:$PC_{71}BM$ BHJ film, (e) MnCl-TPyPAdBr on PCDTBT:$PC_{71}BM$ BHJ film.

Images were collected with a digital camera. As shown in Figure 6(a2–e2), the surfaces of pure PCDTBT:$PC_{71}BM$ and PCDTBT:$PC_{71}BM$ treated by water were largely hydrophobic; their water contact angles were 99.18° and 97.05°, respectively. This result indicates that water treatment only slightly changed the surface polarity of PCDTBT: $PC_{71}BM$. By contrast, the surfaces of PCDTBT: $PC_{71}BM$/ZnTPyP-MeI, Zn-TPyPAdBr, and MnCl-TPyPAdBr were hydrophilic, with respective contact angles of 74.75°, 74.17°, and 71.88°, which suggests accumulation of the ionic component at the topmost organic surface.

The above results revealed accumulation of ionic components at the topmost organic surface and a dipole layer on the surface. The porphyrin-interlayer-induced decrease of the WF of Al also demonstrated the formation of an interfacial dipole layer. The detailed microscopic mechanism of the interfacial dipole remains unclear. However, it is extensively accepted that the interfacial dipole can improve the charge transport, extraction, and V_{oc} of solar cell [3,4, 13–20]. Therefore, PCE increase should be mainly attributed to the formation of interfacial dipole layer in the solar cell.

It is worth noting that Devices 4 and 5 showed better performance than Device 3. A possible explanation for this phenomenon is that in the porphyrin molecules of Zn-TPyPAdBr and MnCl-TPyPAdBr, the relatively large hydrophobic adamant groups may enhance the wettability of the porphyrin interlayer on the active layer, which is beneficial to the charge transport from the active layer to the interlayer. The device performance was sensitive to the thickness of the cathode interlayer. The devices based on the interlayer with thickness of 5 nm displayed the best performance. When the thickness of the cathode interlayer was less than 5 nm, the device performance was poor, which should be attributed to the formation of discontinuous layers of porphyrin. The cathode interlayer with thickness of 7.5 nm was also employed to fabricate a device. Increasing the thickness of the interlayer resulted in an obvious decrease of the device's performance. The thicker interlayer may suppress charge transfer from the active layer to the cathode [39,40].

4 Conclusions

In conclusion, three alcohol/water-soluble porphyrins (Zn-TPyPMeI, Zn-TPyPAdBr, and MnCl-TPyPAdBr) have been synthesized and successfully utilized in the PSCs with PCDTBT:$PC_{71}BM$ as the active layer. Compared with the two control devices, a simultaneous enhancement in V_{oc}, J_{sc}, and FF of the PSCs with porphyrins as cathode interlayers was achieved. A PCE of 6.86% for the device with MnCl-TPyPAdBr interlayer was realized. This PCE value is comparable with the best values of PCE of the PSCs currently reported, which indicates that MnCl-TPyPAdBr is a

promising candidate as a good cathode interlayer for highly efficient PSCs. The porphyrin molecules can induce the vacuum-level shift of an Al cathode via the formation of permanent dipoles at the interface between active layer and metal electrode. For porphyrin molecules, the structural modifidation space is very large. Therefore, optimization of porphyrin molecules should be an efficient strategy to develop organic cathode interlayers for high-performance polymer solar cells by modifing porphyrin molecules.

This work was supported by the National Basic Research Program of China (2014CB643500) and the National Natural Science Foundation of China (51273077, 51173065).

1 Chen HY, Hou JH, Zhang SQ, Liang YY, Yang GW, Yang Y, Yu LP, Wu Y, Li G. Polymer solar cells with enhanced open circuit voltage and efficient. *Nat Photonic*, 2009, 3: 649–653
2 Ye L, Zhang SQ, Zhao WC, Yao HF, Hou JH. Highly efficient 2D-conjugated benzodithiophene-based photovoltaic polymer with linear alkylthio side chain. *Chem Mater*, 2014, 26: 3603–3605
3 He ZC, Zhong CM, Su SJ, Xu M, Wu HB, Cao Y. Enhanced power-conversion efficiency in polymer solar cells using an inverted device structure. *Nat Photonic*, 2012, 6: 591–595
4 He ZC, Zhong C, Huang X, Wong WY, Wu H, Chen L, Su S, Cao Y. Simultaneous enhancement of open-circuit voltage, short-circuit current density, and fill factor in polymer solar cells. *Adv Mater*, 2011, 23: 4636–4643
5 Liang Y, Xu Z, Xia J, Tsai ST, Wu Y, Li G, Ray C, Yu L. For the bright future—bulk heterojunction polymer solar cells with power conversion efficiency of 7.4%. *Adv Mater*, 2010, 22: E135–E138
6 Huo L, Zhang S, Guo X, Xu F, Li Y, Hou J. Replacing alkoxy groups with alkylthienyl groups: a feasible approach to improve the properties of photovoltaic polymers. Ang*ew Chem Int Ed*, 2011, 50: 9697–9702
7 Deng Y, Liu J, Wang J, Liu L, Li W, Tian H, Zhang X, Xie Z, Geng Y, Wang F. Dithienocarbazole and isoindigo based amorphous low bandgap conjugated polymers for efficient polymer solar cells. *Adv Mater*, 2013, 3: 471–476
8 Gao L, Zhang J, He C, Zhang Y, Sun QJ, Li YF. Effect of additives on the photovoltaic properties of organic solar cells based on triphenylamine-containing amorphous molecules. *Sci China Chem*, 2014, 57: 966–972
9 Liu X, Cai P, Chen DC, Chen JW, Su SJ, Cao Y. Small molecular non-fullerene electron acceptors for P3HT-based bulk-heterojunction solar cells. *Sci China Chem*, 2014, 57: 973–981
10 Liu J, Shao S, Fang G, Meng B, Xie Z, Wang L. High-efficiency inverted polymer solar cells with transparent and work-function tunable MoO_3-Al composite film as cathode buffer layer. *Adv Mater*, 2012, 24: 2774–2779
11 Yang TB, Qin DH, Lan LF, Huang WB, Gong X, Peng JB, Cao Y. Inverted polymer solar cells with a solution-processed zinc oxide thin film as an electron collection layer. *Sci China Chem*, 2012, 55: 755–759
12 Jo J, Na SI, Kim SS, Lee TW, Chung Y, Kang SJ, Vak D, Kim DY. Three-dimensional bulk heterojunction morphology for achieving high internal quantum efficiency in polymer solar cells. *Adv Funct Mater*, 2009, 19: 2398–2406
13 Tang Z, Andersson LM, George Z, Vandewal K, Tvingstedt K, Heriksson P, Kroon R, Andersson MR, Inganäs O. Interlayer for modified cathode in highly efficient inverted ITO-free organic solar cells. *Adv Mater*, 2012, 24: 554–558
14 Oh SH, Na SI, Jo J, Lim B, Vak D, Kim DY. Water-soluble polyfluorenes as an interfacial layer leading to cathode-independent high performance of organic solar cells. *Adv Funct Mater*, 2010, 20: 1977–1983
15 Zhao Y, Xie Z, Qin C, Qu Y, Geng Y, Wang L. Enhanced charge collection in polymer photovoltaic cells by using an enthanol-soluble conjugated polyfluorene as cathode buffer layer. *Sol Energ Mat Sol C*, 2009, 93: 604–608
16 Seo JH, Gutacker A, Sun Y, Wu H, Huang F, Cao Y, Scherf U, Heeger AJ, Bazan GC. Improved high-efficiency organic solar cells via incorporation of a conjugated polyelectrolyte interlayer. *J Am Chem Soc*, 2011, 133: 8416–8419
17 Chang YM, Zhu R, Richard E, Chen CC, Li G, Yang Y. Electrostatic self-assembly conjugated polyelectrolyte-surfactant complex as an interlayer for high performance polymer solar cells. *Adv Funct Mater*, 2012, 22: 3284–3289
18 Li SS, Lei M, Lv ML, Watkins SE, Tan ZA, Zhu J, Hou JH, Chen XW, Li YF. [6,6]-Phenyl-C61-butyric acid dimethylamino ester as a cathode buffer layer for high-performance polymer solar cells. *Adv Energy Mater*, 2013, 3: 1569–1574
19 Ye H, Hu X, Jiang Z, Chen D, Liu X, Nie H, Su SJ, Gong X, Cao Y. Pyridinium salt-based molecules as cathode interlayers for enhanced performance in polymer solar cells. *J Mater Chem A*, 2013, 1: 3387–3394
20 Vasilopoulou M, Georgiadou DG, Douvas AM, Soultati A, Constantoudis V, Davazoglou D, Gardelis S, Palilis LC, Fakis M, Kennou S, Lazarides T, Coutsolelos AG, Argitis P. Porphyin oriented self- assembled nanostructures for efficient exciton dissociation in high-performing organic photovoltaics. *J Mater Chem A*, 2014, 2: 182–192
21 Zhou J, Wan X, Liu Y, Zuo Y, Li Z, He G, Long G, Ni W, Li C, Su X, Chen Y. Small molecules based on benzo[1,2-b:4,5-b′]dithiophene unit for high-performance solution-processed organic solar cells. *J Am Chem Soc*, 2012, 134: 16345–16351
22 Tsuda A, Osuka A. Fully conjugated porphyrin tapes with electronic absorption bands that reach into infrared. *Science*, 2001, 293: 79–82
23 Zhang H, Zhang B, Zhu M, Grayson SM, Schmehl R, Jayawickramarajah J. Water-soluble porphyrin nanospheres: enhancedphotophysical properties achieved viacyclodextrin driven double self-inclusion. *Chem Commun*, 2014, 50: 4853–4855
24 Dong RJ, Bo Y, Tong G, Zhou Y, Zhu X, Lu Y. Self-assembly and optical properties of a porphyrin-based amphiphile. *Nanoscale*, 2014, 6: 4544–4550
25 Huo C, Zhang HD, Zhang HY, Zhang HY, Yang B, Zhang P, Wang Y. Synthesis and assembly with mesoprous silica MCM-48 of platinum prophyrin complexes bearing carbazeyl groups: spectroscopic and oxygen sensing properties. *Inorg Chem*, 2006, 45: 4735–4742
26 Bhyrappa P, Young JK, Moore JS, Suslick KS. Dendrimer-metalloporphyrins: synthesis and catalysis. *J Am Chem Soc*, 1996, 118: 5708–5711
27 Fateeva A, Chater PA, Ireland CP, Tahir AA, Khimyak YZ, Wiper PV, Darwent JR, Rosseinsky MJ. A water-stable porphyrin-based metal-organic framework active for visible-light photocatalysis. *Angew Chem Int Ed*, 2012, 124: 7558–7562
28 Janghouri M, Mohajerani E, Amini MM, Safari N. Porphyrin doping of dichloride-bis(5,7-dichloroquinolin-8-olato)tin (IV) complex for electroluminescence. *J Porphyr Phthalocya*, 2013, 17: 351–358
29 Graham KR, Yang Y, Sommer JR, Shelton AH, Schanze KS, Xue J, Reynolds JR. Extended conjugation platinum prophyrins for use in near-infrared emitting organic light emitting diodes. *Chem Mater*, 2011, 23: 5305–5312
30 Mathew S, Yella A, Gao P, Humphry-Baker R, Curchod BE, Ashari-Astani N, Tavernelli I, Rothlisberger U, Nazeeruddin MK , Grtäzel M. Dye-sensitized solar cells with 13% efficiency achieved through the molecular engineering of porphyrin sensitizers. *Nat Chem*, 2014, 6: 242–247
31 Luechai A, Gasiorowski J, Petsom A, Neugebauer H, Sariciftci NS, Thamyongkit P. Photosensitizing porphyrin-triazine compound for bulk heterojunction solar cells. *J Mater Chem*, 2012, 22: 23030–23037
32 Singh VK, Kanaparthi RK, Giribabu L. Emerging molecular design strategies of unsymmetrical phthalocyanines for dye-senstitized solar

cell applications. *RSC Adv*, 2014, 4: 6970–6984
33 Wu C, Chen M, Su P, Kuo H, Wang C, Lu C, Tsai C, Wu C, Lin C. Porphyrins for efficient dye-sensitized solar cells covering the near-IR region. *J Mater Chem A*, 2014, 2: 991–999
34 Zervaki GE, Papastamatakis E, Angaridis PA, Nikolaou V, Singh M, Kurchania R, Kitsopoulos TN, Sharma GD, Coutsolelos AG. A propeller-shaped, triazine-linked porphyrin triad as efficient sensitizer for dye-sensitized solar cells. *Eur J Inorg Chem*, 2014, 6: 1020–1033
35 Vasilopoulou M, Georgiadou DG, Douvas AM, Soultati A, Constantoudis V, Davazoglou D, Gardelis S, Palilis LC, Fakis M, Kennou S, Lazarides T, Coutsolelosd AG, Argitis P. Porphyrin oriented self-assembled nanostructures for efficient exciton dissociation in high-performing organic photovoltaics. *J Mater Chem A*, 2014, 2: 182–192
36 Zervaki GE, Roy MS, Panda MK, Angaridis PA, Chrissos E, Sharma GD, Coutsolelos AG. Efficient sensitization of dye-sensitized solar cells by novel triazine-bridged porphyrin-porphyrin dyads. *Inorg Chem*, 2013, 52: 9813–9825
37 Sharmaa GD, Daphnomili D, Biswas S, Coutsolelos AG. New soluble porphyrin bearing a pyridinylethynyl group as donor for bulk heterojunction solar cells. *Org Electronics*, 2013, 14: 1811–1819
38 Choi S, Chae SH, Hoang MH, Kim KH, Huh JA, Kim Y, Kim SJ, Choi DH, Lee SJ. An unsymmetrically π-extended porphyrin-based single-crystal field-effect transistor and its anisotropic carrier-transport behavior. *Chem Eur J*, 2013, 19: 2247–2251
39 Zhang ZG, Li H, Qi BY, Chi D, Jin ZW, Qi Z, Hou JH, Li YF, Wang JZ. Amine group functionalized fullerene derivatives as cathode buffer layers for high performance polymer solar cells. *J Mater Chem A*, 2013, 1: 9624–9629
40 Zhang ZG, Hui H, Qi Z, Jin ZW, Liu G, Hou JH, Li YF, Wang JZ. Poly(ethylene glycol) modified [60]fullerene as electron buffer layer for high-performance polymer solar cells. *Appl Phys Lett*, 2013, 102: 143902